Monitoring of active galactic nuclei[*]

IV. The Seyfert 1 galaxy NGC 4593

M. Dietrich[1], W. Kollatschny[1], D. Alloin[2], I. Aretxaga[3], D. Axon[4,10], A.G. de Bruyn[5], J. Clavel[6], M.R. Goad[7], P. Gondhalekar[8], E. van Groningen[9], K. Horne[10], N. Jackson[11], E. Laurikainen[12], A. Lawrence[13], J. Masegosa[14], M. Moles[14], P. O'Brien[7], A. del Olmo[14], M.V. Penston[15,**], J. Perea[14], E. Pérez[16], I. Pérez-Fournon[16], J.J. Perry[17], B.M. Peterson[18], A. Robinson[17], J.M. Rodríguez Espinosa[16], G.M. Stirpe[19], C. Tadhunter[20], R. Terlevich[15], S. Unger[15], S.J. Wagner[21], I. Wanders[9], and R. Williams[17]

[1] Universitäts-Sternwarte, Geismarlandstraße 11, D-37083 Göttingen, Germany
[2] observatoire de Paris, URA 173 CNRS, Université Paris 7, Place Jules Janssen, F-92195 Meudon Principal Cedex, France
[3] Dpto. Física Teórica, C-XI, Universidad Autónoma de Madrid, E-28049 Madrid, Spain
[4] NRAL, Jodrell Bank, Macclesfield, Cheshire SK11 9DL, UK
[5] Radiosterrewacht, Postbus 2, NL-7990 AA Dwingeloo, The Netherlands
[6] ESA Astrophysics Division, ESTEC, Postbus 299, NL-2200 AG Noordwijk, The Netherlands
[7] Department of Physics and Astronomy, UCL, Gower Street, London WC1E 6BT, UK
[8] Rutherford Appleton Laboratory, Chilton, Didcot, Berks OX1 0QX, UK
[9] Astronomiska observatoriet, Box 515, S-75120 Uppsala, Sweden
[10] Space Telescope Science Institute, 3700 San Martin Drive, Baltimore, MD 21218, USA
[11] Sterrewacht Leiden, Postbus 9513, NL-2300 RA Leiden, The Netherlands
[12] Turku University Observatory, Tuorla, SF-21500 Piikkiö, Finland
[13] Queen Mary College, University of London, Mile End Road, London E1, UK
[14] Instituto de Astrofísica de Andalucía, CSIC, Apartado 3004, E-Granada, Spain
[15] Royal Greenwich Observatory, Madingley Road, Cambridge CB3 0EZ, UK
[16] Instituto de Astrofísica de Canarias, E-38200 La Laguna, Tenerife, Spain
[17] Institute of Astronomy, Madingley Rd., Cambridge CB3 0HA, UK
[18] Department of Astronomy, Ohio State University, 174 West 18th Avenue, Columbus, OH 43210, USA
[19] Osservatorio Astronomico di Bologna, Via Zamboni 33, I-40126 Bologna, Italy
[20] Department of Physics, Hounsfield Rd., Sheffield S3 73H, UK
[21] Landessternwarte Königstuhl, D-69117 Heidelberg, Germany

Abstract. Results of a five-month campaign of optical monitoring the Seyfert 1 galaxy NGC 4593 are presented. High resolution Hα and Hβ spectra and direct images in the Johnson U, B, V, R and I bands were obtained between January and June 1990. The emission lines and the continuum showed strong variations on time scales of weeks to days. The Hα line varied by more than 30 % within only 5 days. Cross-correlating the light curves of the Balmer lines with that of the optical continuum gives a lag of around 4 days. Therefore, this low luminosity Seyfert galaxy may have one of the smallest BLRs known so far.

Key words: galaxies: individual: NGC 4593 – galaxies: Seyfert – lines: profile

1. Introduction

Variability on time scales of weeks to years has been detected in several Seyferts and QSOs in both the optical continuum and the emission lines, following the first observations of Dibaj & Pronik (1967) and Andrillat & Souffrin (1968). The intensity variations are observed not only in the optical but also at all other observed frequencies from X-ray to radio.

In the past 5 years it has become clear that Seyfert galaxies vary in the optical on time scales as short as a few days. For NGC 4151 and NGC 5548 delays of 4 to 18 days have been detected for optical and UV emission lines with respect to continuum variations (Clavel et al. 1990, 1991; Netzer et al. 1990; Peterson et al. 1991, 1992; Dietrich et al. 1993). A coordinated monitoring programme was started within the LAG (Lovers of Active Galaxies, cf. van Groningen & Wanders 1993) collaboration (Jackson et al. 1992; Wanders et al. 1993; Salamanca et al. 1993) to study the short term variability in AGN on time scales of days for a period of 6 months; one of the programme galaxies was NGC 4593. It is a nearby ($v_0 = 2505$ km s^{-1}) barred spiral galaxy of Hubble type SBb. NGC 4593 is affected by the gravitational field of the Virgo cluster although it is not a cluster member. Galaxies beyond the cluster show smaller redshift than those corresponding to isotropic Hubble flow. Taking into account models for the infall of the Local Group into Virgo (Whittle 1992) the corrected recession velocity of NGC 4593 is 2700 km s^{-1} depending on the adopted parameters for the Local Group infall and the redshift of the Virgo cluster.

Its apparent magnitude, $V_T = 13.15$, corresponds to an absolute V magnitude of $M_V = -20.5$ ($H_0 = 50$ km s^{-1} Mpc^{-1}, $v_0 = 2505$ km s^{-1}) (Véron-Cetty & Veron 1991). NGC 4593 contains a Seyfert 1 nucleus and is a member of a group of 5 galaxies (Kollatschny & Fricke 1989).

Variations of the UV continuum flux and emission lines in NGC 4593 on time scales of months as well as 30 % variations within nine days (Clavel 1983) have been published. IUE observations from 1983 to 1986 showed significant variations within a few days (Santos-Lleó et al. 1990; Koratkar & Gaskell 1991a). Variations of the Balmer lines and of the optical continuum on time scales of months to years were found by Peterson et al. (1985). Between March 1982 (Kollatschny & Fricke 1985) and March 1990 the flux of the broad Hβ component has decreased by 50 %.

Variations in the IR bands J, H, K and L on time scales of days were observed in February 1985 (Santos-Lleó et al. 1990). Furthermore, the amplitude of the variations decreased with increasing frequency. These IR variations were not correlated with the variations in the UV.

Very rapid X-ray variations within hours were detected with Exosat (Barr et al. 1987). The X-ray flux is correlated with the UV flux on medium to long time scales but no correlations were found on time scales shorter than 1 day (Santos-Lleó et al. 1990).

All these earlier observations of NGC 4593 pointed to this galaxy as a prime candidate for short time-scale variability investigations.

2. Observations and data analysis

2.1. Spectroscopy

NGC 4593 was observed spectroscopically on several occasions between January and June 1990 with the 4.2m William Herschel Telescope (WHT) and the 2.5m Isaac Newton Telescope (INT) at La Palma, Spain.

The ISIS spectrograph was mounted at the WHT while the IDS spectrograph was attached to the INT. The 500 mm camera and an EEV CCD were used at the WHT while the 235 mm as well as the 500 mm camera and the GEC CCD were used at the INT. The spatial resolution of the spectra corresponds to $0\farcs335$/pxl at the WHT and $0\farcs646$/pxl or $0\farcs304$/pxl depending on which camera was used, at the INT. The gratings were selected to maximize resolution while yielding a wavelength coverage of ~ 900 Å. We fixed the slit width to $1\farcs5$ projected on the sky for all spectra, except on April 2nd, when the slit width was $1\farcs9$. The position angle of the slit was set to PA=0° throughout the campaign. A journal of the observations is given in Table 1: column (1) gives the year, month and day of the observation, column (2) the Julian date -2440000, (3) the telescope and (4) the camera; (5) the dispersion of the spectra in units of [Å/pxl], (6) the corresponding wavelength range, (7) the exposure time in units of seconds and (8) the seeing value in units of arcsec. CuNe or CuAr spectra were taken after each object exposure for wavelength calibration. Spectra of the standard stars BD+26° 2606 and HD84937 were observed for flux calibration (Barnes & Hayes 1984; Oke & Gunn 1983; Oke 1990).

Tungsten lamp flat field exposures were taken before or after each observing night. The 2D-spectra were corrected for bias and dark current. Cosmic-ray events were identified by inspection of the raw images, and were removed by interpolating across the affected regions.

The night sky in the 2D-spectra was subtracted by fitting Legendre polynomials of third order perpendicular to the dispersion. These polynomials were fitted on each row of the spectra using areas on both sides of the object spectrum which were not contaminated by the galaxy.

We corrected the object spectrum for the atmospheric B-band from 6850 to 6900 Å in the following way. The absorption feature was linearly interpolated in the spectrum of the standard stars which were observed under the same conditions. The ratio between the interpolated and original spectrum gives the scaling factors for the correction of the atmospheric B-band absorption.

The spatial extraction window of the spectra was set to $3\farcs0$. Therefore, the integration aperture amounted to $3\farcs0 \times 1\farcs5$. This aperture is sufficient to allow use of the narrow forbidden emission lines for the internal calibration of the spectra since the NLR of NGC 4593 is spatially unresolved (Enrique Pérez, priv.comm.). Furthermore, we compared the spatial profiles of the broad Hβ line and of the narrow [O III]$\lambda\lambda4959,5007$ emission lines. The profiles have been corrected with respect to the stellar contribution of the galaxy. The spatial profiles of the broad Hβ line and of the [O III] lines are identical. Therefore, the BLR and the NLR of NGC 4593 are spatially unresolved. We also tested the influence of different spatial extraction windows on the line intensity measurements. With an extraction window of $5\farcs0 \times 1\farcs5$ the flux of the broad and narrow emission lines remained constant within 2 %. Only the contribution of the stellar component was stronger in the spectra with the larger aperture. The calibrated 1D spectra were rebinned with a step size of 1

Table 1. Observational log of the NGC 4593 spectroscopic monitoring campaign

date (1)	jul.date (2)	tel. (3)	cam. (4)	disp. (5)	$\lambda\lambda$ (6)	exp. (7)	see. (8)
89:12:31	7891.701	OSU	CCDS	2.00	Hβ	2400	5.4
90:01:02	7894.728	INT	235	1.45	Hα	1000	2.3
90:01:05	7897.685	INT	235	1.45	Hα	1000	1.5
90:01:10	7901.637	OSU	CCDS	2.00	Hβ	3600	3.9
90:01:10	7902.644	INT	235	1.45	Hα	1000	1.8
90:01:19	7911.677	INT	500	1.45	Hα	1200	2.2
90:01:19	7911.737	WHT	500	0.73	Hα	500	2.6
90:01:24	7916.721	WHT	500	0.73	Hα	350	2.1
90:01:28	7920.735	INT	500	1.45	Hα	1000	1.8
90:01:31	7923.672	WHT	500	0.73	Hβ	700	1.1
90:01:31	7923.681	WHT	500	0.73	Hα	350	1.3
90:02:05	7928.688	INT	500	1.45	Hα	1000	1.9
90:02:08	7931.654	INT	500	1.45	Hα	1000	1.5
90:02:11	7934.570	INT	500	1.45	Hα	1000	4.8
90:02:16	7939.625	WHT	500	0.73	Hα	400	1.1
90:02:21	7944.666	INT	235	1.45	Hα	1000	2.6
90:03:06	7957.554	INT	235	1.45	Hα	1000	2.3
90:03:06	7957.568	INT	235	1.45	Hβ	2400	2.1
90:03:17	7968.633	WHT	500	0.73	Hβ	1000	1.3
90:03:17	7968.653	WHT	500	0.73	Hα	1000	1.5
90:04:02	7984.508	WHT	500	0.73	Hα	350	1.6
90:04:02	7984.508	WHT	500	1.40	Hβ	600	1.6
90:04:13	7995.519	INT	500	1.45	Hα	1000	2.5
90:04:15	7997.500	INT	500	1.45	Hα	1700	3.0
90:05:02	8014.447	WHT	500	0.73	Hβ	700	0.9
90:05:02	8014.463	WHT	500	0.73	Hα	350	1.1
90:05:13	8025.472	WHT	500	0.73	Hβ	700	1.3
90:05:13	8025.490	WHT	500	0.73	Hα	350	1.2
90:05:15	8027.581	INT	235	1.45	Hα	1000	2.8
90:05:19	8031.639	INT	235	1.45	Hα	1000	1.3
90:05:24	8036.543	WHT	500	0.73	Hα	350	1.7
90:05:26	8037.750	OSU	CCDS	2.00	Hβ	3600	4.4
90:06:02	8044.731	OSU	CCDS	2.00	Hβ	3600	2.6
90:06:06	8049.463	INT	500	1.45	Hβ	2400	1.9
90:06:06	8049.495	INT	500	1.45	Hα	1600	2.4

Å to a uniform wavelength range of 4500 to 5400 Å (blue) and 6200 to 7200 Å (red).

We obtained Hα spectra at 23 epochs and Hβ at 7 epochs. Four additional spectra covering the Hβ spectral region were obtained with the OSU CCD spectrograph on the 1.8 m Perkins Telescope of the Ohio State and Ohio Wesleyan Universities at the Lowell Observatory near Flagstaff, Arizona. These data were obtained through a larger aperture (5″x6″) than were the WHT or INT data; however, as discussed below, neither the NLR nor the BLR appear to be spatially resolved in this source, so the Hβ fluxes derived from these data should not show any differences due to aperture effects.

For the Hα light curve we used spectra of only 22 epochs, since for one epoch (JD 2447934) the S/N was insufficient to measure the flux in a reliable way.

In the period from March to May, the sampling rate was not as good as in the beginning of the monitoring campaign: the sampling rate of the first half of the monitoring campaign (JD 2447894 to ...7968) was 4.2 days and that of the second half was 11 days. The mean sampling rate of the Hα spectra of the entire monitoring campaign was 7.1 days.

The narrow forbidden lines originate in the spatially more extended narrow-line region and are considered to be constant on time scales of at least 10 years. Therefore, we scaled the spectra of the broad Hα component with respect to the [O I]$\lambda\lambda$6300,6364, [S II]$\lambda\lambda$6717,6731, [N II]$\lambda\lambda$6548,6584 and narrow Hα lines, while Hβ was scaled with respect to the [O III]$\lambda\lambda$4959,5007 lines.

The spectra have to be corrected for small spectral shifts, slightly different spectral resolutions and scaling factors with respect to one reference spectrum. The parameters scaling factor, wavelength shift and dispersion correction were varied interactively until the residuals of the narrow emission lines were minimized, as judged by eye. This procedure is similar to the one described by van Groningen & Wanders (1992). The normalized spectra of the Hα and Hβ emission lines are shown in Fig. 1 and 2.

We also tested the possible influence of the seeing on our flux measurements. We measured the seeing of each object spectrum in the following way. The spatially unresolved broad line fluxes of the blue and red wings of the Hα line were averaged perpendicular to the dispersion. The same procedure was used for the continuum flux near the broad emission line. The profile of the spatially averaged continuum was subtracted from the profile of the broad emission line flux. The resulting spatial profile represents only the unresolved broad emission line flux since the contribution of the stellar component is contained in both profiles and cancels out. We derived the seeing by measuring the full width at half maximum (FWHM) of these profiles directly. The resulting seeing values are given in Table 1. These seeing values are not correlated with the intensity variations of the Hα or Hβ emission lines.

Since we took Hα spectra with two different telescopes we examined the data for possible systematic differences. For one epoch, January 19th, spectra were taken nearly simultaneously with both telescopes. The temporal separation was 86 minutes. Differences in the spectra should lead to small scale structures in the profile of the difference spectrum (Fig. 3). There are no structures visible in this spectrum. The difference in the integrated Hα emission line of these two epochs amounts to only 0.4 % of the total flux. The uncertainties in the flux measurements that may be introduced by using different telescopes and instruments are less than 3 %, which is much less than the relative amplitude of the flux variations (e.g. Fig. 4).

2.2. Photometry

Broad band differential photometry in the Johnson U, B, V, R, and I bands was obtained at the 1.0m Jacobus Kapteyn Telescope (JKT) at La Palma. Usually the GEC P8603 CCD chip was attached at the JKT, yielding a scale of 0″30 /pxl. At three
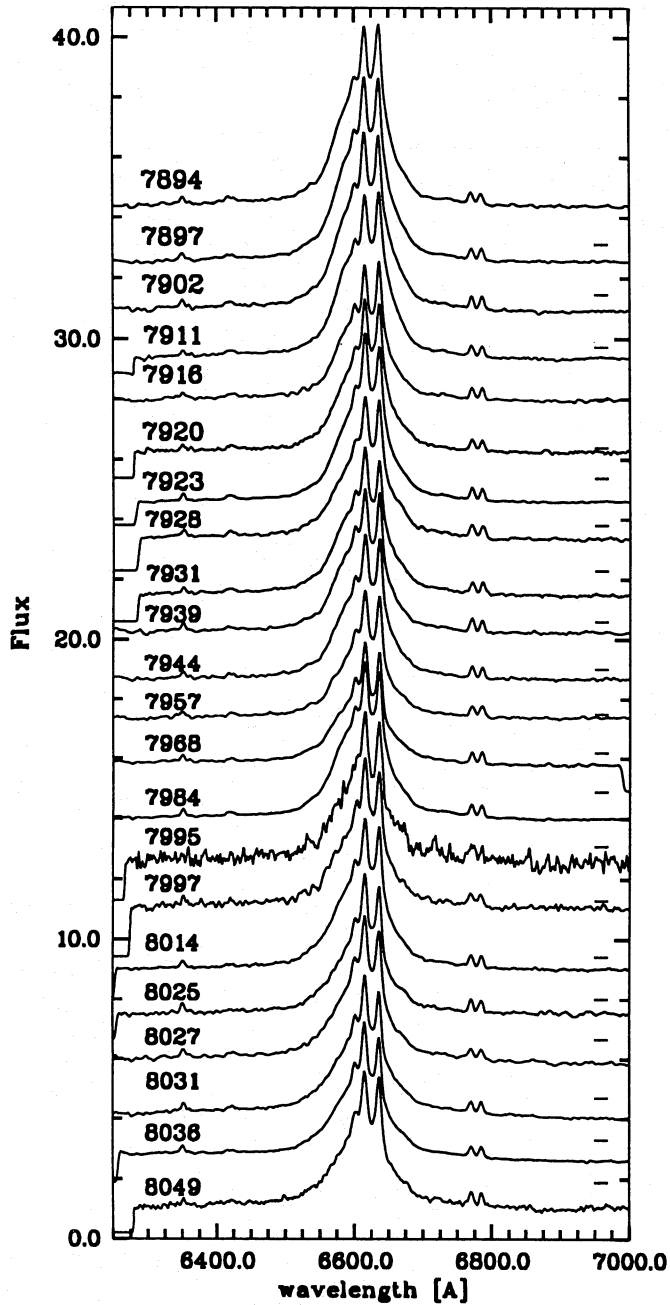
Fig. 1. Hα spectra from JD = 2447894 until 2448049; the flux is given in units of 10^{-14} erg s^{-1} cm^{-2} Å^{-1}; the tick marks indicate the corresponding zero level for the displayed spectra

epochs an RCA SID501 CCD chip was used (0.″41 /pxl). The area of the sky covered by the two detectors was 115″ x 173″ and 130″ x 210″, respectively. NGC 4593 was not positioned exactly in the centre of the field in order to obtain at least one foreground star on the CCD frame for flux calibration. In Table 2 we list the observing dates, the CCD chips, the exposure times of the B-band observations, the seeing measured in the B-band images and the filters used.

After dark-current and bias subtraction the frames were flat field corrected using observed sky flat images as well as dome
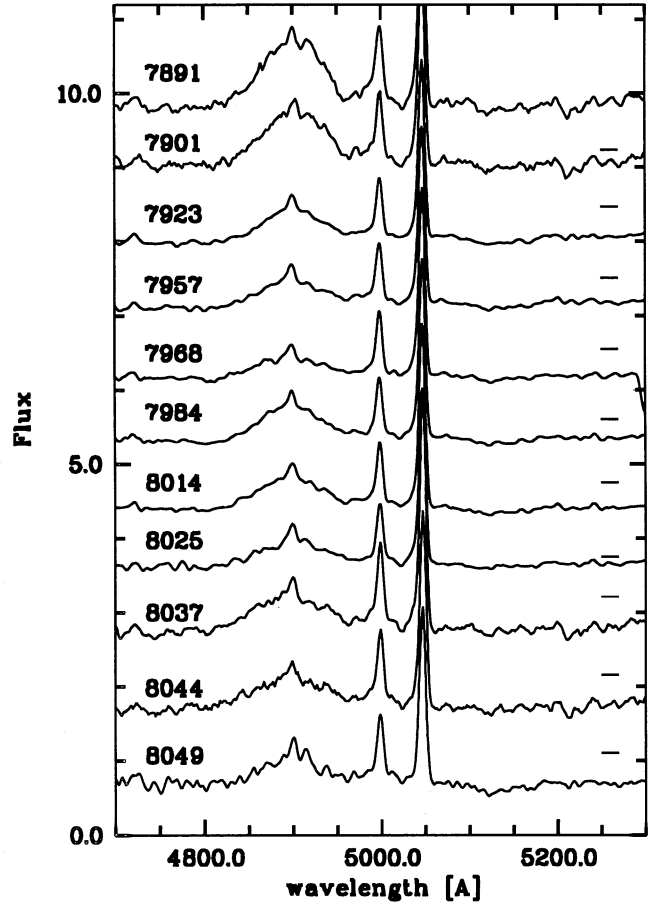
Fig. 2. Hβ spectra from JD = 2447891 until 2448049; the flux is given in units of 10^{-14} erg s^{-1} cm^{-2} Å^{-1}; the tick marks indicate the corresponding zero level for the displayed spectra

Table 2. Observational log of the NGC 4593 photometric monitoring campaign of 1990; the exposure time in units of seconds and the seeing values in arcsec refer to the B-band images

| date	Jul.date	dev.	exp.	see.	U	B	V	R	I
0201	7894.762	GEC	300	2.0	-	x	x	x	x
1501	7907.609	GEC	360	3.8	-	x	x	x	x
1501	7907.619	GEC	360	4.3	-	x	-	-	x
1801	7910.765	RCA	350	2.1	-	x	x	x	x
2401	7916.624	RCA	480	2.8	-	x	-	x	x
3101	7923.679	RCA	480	1.6	-	x	-	x	x
0502	7928.613	GEC	480	1.9	-	x	x	x	x
0802	7931.572	GEC	480	1.2	x	x	x	x	x
1102	7934.694	GEC	480	2.2	x	x	x	x	x
1602	7939.628	GEC	480	1.6	x	x	-	x	x
2102	7944.697	GEC	480	3.1	x	x	-	x	x
1003	7961.651	GEC	480	1.2	x	x	x	x	x
1303	7964.533	GEC	480	2.5	x	x	x	x	x
2904	8011.549	GEC	480	1.6	x	x	x	x	x
1805	8030.538	GEC	480	1.9	x	x	-	x	x
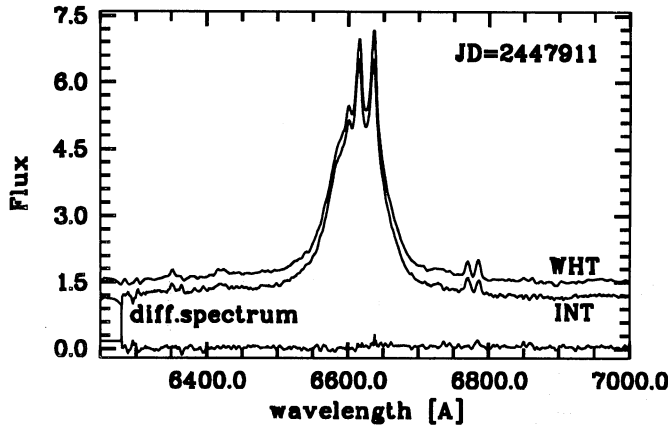
Fig. 3. Comparison of two Hα spectra obtained during the same night (JD=2447911) with the 4.2m WHT (top) and the 2.5m INT (bottom). An offset has been added to the spectra for display purposes. The difference between the two spectra is also shown

Fig. 4. Light curve of Hα. The intensity is given in units of 10^{-14} erg s^{-1} cm^{-2} and includes the constant contribution of the narrow component of Hα and the [N II]$\lambda\lambda6548,6584$ lines

flat images. The sky subtraction in the images was performed by fitting polynomials of second or third order to the background. These background fits were subtracted from the frames.

3. Emission-line and continuum light curves

3.1. Hα and Hβ emission-line light curves

The intensity of the Hα line was determined from the internally calibrated spectra by integrating the flux above the continuum interpolating between 6450 to 6800 Å, corresponding to 6398 to 6746 Å in the rest frame of NGC 4593. The light curve of the variable broad Hα line intensity is shown in Fig. 4. The fluxes of the narrow emission lines [N II]$\lambda\lambda6548,6584$ and Hα$_{narrow}$ and the variable broad Hα emission line flux are included in the measurements given in Table 3. We integrated the Hβ line flux from 4800 to 5000 Å and scaled the flux with respect to the forbidden [O III]$\lambda\lambda4959,5007$ emission lines. The integrated Hβ flux includes the variable broad component as well as the constant narrow one. Since the narrow line flux components are constant in time the pattern of the light curve remains unchanged. The uncertainty in the Hα and Hβ emission line flux measurements is of the order of 3%. The individual errors given in Tables 3 and 4 are derived from the scatter of the narrow line flux measurements of [S II]$\lambda\lambda6717,6731$, [N II]$\lambda\lambda6548,6584$, [O III]$\lambda\lambda4959,5007$, Hα$_{narrow}$ and Hβ$_{narrow}$. The flux intensities of the narrow lines are given in Table 4. The emission line fluxes of Hβ$_{narrow}$, [O III]$\lambda\lambda4959,5007$ and [S II]$\lambda\lambda6717,6731$ were measured directly. In order to measure the line intensity of Hα$_{narrow}$ and [N II]$\lambda\lambda6548,6584$ we have deconvolved the line profile for those epochs of Hα when NGC 4593 was in a lower activity phase. The best fit to the Hα complex was obtained by using five Gaussian components, with two separate components to fit the variable broad lines and three to fit the constant narrow features, Hα$_{narrow}$ and the [N II] lines. The fit parameters are given in Table 5.

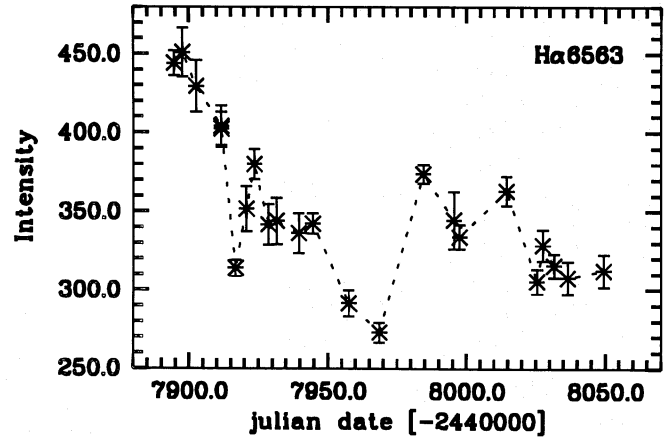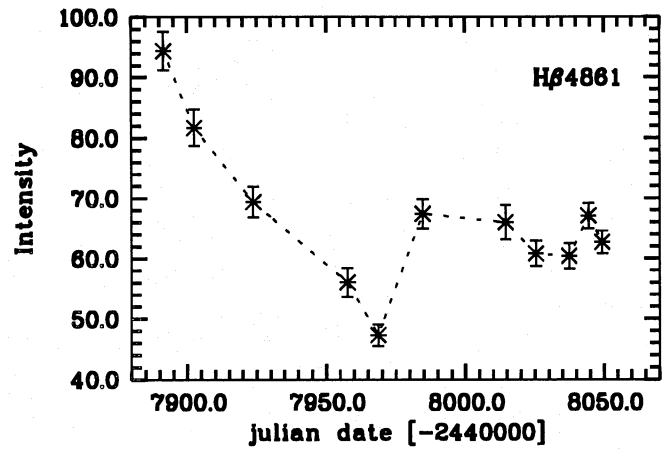**Fig. 5.** Light curve of Hβ. The intensity is given in units of 10^{-14} erg s^{-1} cm^{-2} and includes the constant contribution of the narrow line component of Hβ

The absolute flux calibration was done by comparing the measured narrow line fluxes of [S II]$\lambda\lambda6717,6731$ and [O III]$\lambda\lambda4959,5007$ with the results given by Clavel et al. (1983) and Kollatschny & Fricke (1985).

The integrated Hα intensity declined from January to the beginning of March (JD 2447894 until JD 2447968). A spectacular event occurred during the second half of January. Within only 5 days the Hα flux dropped by 30 %. During the following seven days the flux increased again and reached nearly the same intensity level as at the beginning of this short time variation. From the minimum state (JD 2447968) the flux rose again by 30 % and then declined to a relatively low state at the end of the monitoring campaign.

The light curve of the broad Hβ emission line has a sparse temporal coverage in comparison to that of Hα. In spite of the lower sampling rate the light curve of the varying broad Hβ flux shows a variability pattern remarkably similar to that of the Hα line (cf. Fig. 4 and 5). The rapid variation during the second

Table 3. Observed Balmer line intensities and continuum fluxes. The intensities of the emission lines are given in units of 10^{-14} erg s^{-1} cm^{-2}, the continuum flux F_{6310} in units of 10^{-15} erg s^{-1} cm^{-2} Å^{-1}. The flux in the B band is normalized with respect to the mean flux.

Jul.date	Hα	Hβ	F_{6310}	F_{B-band}
7891.701	—	94.4±3.2	—	—
7894.730	444.1± 8.0	—	11.38±0.52	—
7897.685	451.0±15.8	—	11.38±0.52	—
7901.637	—	81.7±3.0	—	—
7902.644	429.5±16.3	—	10.19±0.52	—
7907.609	—	—	—	1.16±0.04
7907.619	—	—	—	1.11±0.04
7910.765	—	—	—	1.08±0.04
7911.677	404.0±13.3	—	9.15±0.52	—
7911.737	402.5±10.5	—	9.04±0.52	—
7916.721	313.8± 5.3	—	7.69±0.52	0.82±0.04
7920.735	351.6±14.4	—	8.27±0.52	—
7923.672	—	69.4±2.5	—	—
7923.681	380.1± 9.5	—	9.01±0.52	0.89±0.04
7928.688	341.6±13.0	—	9.43±0.52	0.97±0.04
7931.654	343.9±14.8	—	8.68±0.52	1.07±0.04
7934.694	—	—	—	1.05±0.04
7939.625	336.2±12.8	—	8.51±0.52	1.06±0.04
7944.666	342.3± 6.5	—	8.02±0.52	0.97±0.04
7957.554	291.4± 8.2	—	6.76±0.52	—
7957.568	—	56.0±2.4	—	—
7961.651	—	—	—	0.96±0.04
7964.533	—	—	—	0.86±0.04
7968.633	—	47.3±1.8	—	—
7968.653	272.9± 6.3	—	8.07±0.52	—
7984.508	373.9± 6.0	67.4±2.4	8.64±0.52	—
7995.520	344.5±18.2	—	7.62±0.52	—
7997.500	333.8± 7.7	—	7.53±0.52	—
8011.549	—	—	—	0.90±0.04
8014.447	—	66.0±2.9	—	—
8014.463	363.1± 9.4	—	8.15±0.52	—
8025.472	—	60.8±2.1	—	—
8025.490	305.4± 7.9	—	8.35±0.52	—
8027.581	328.4± 9.9	—	8.04±0.52	—
8030.538	—	—	—	0.90±0.04
8031.639	315.4± 7.6	—	8.10±0.52	—
8036.543	307.6±10.2	—	8.32±0.52	—
8037.750	—	60.4±2.1	—	—
8044.731	—	67.1±2.1	—	—
8049.463	—	62.7±1.9	—	—
8049.495	312.2±10.3	—	8.49±0.52	—

Table 4. Observed narrow line fluxes; the intensities of the emission lines are given in units of 10^{-14} erg s^{-1} cm^{-2}

Feature	Flux
Hβ$_{narrow}$	2.49±0.25
[O III]λ4959	8.30±0.20
[O III]λ5007	24.64±0.57
[N II]λ6548	4.56±0.44
Hα$_{narrow}$	15.80±0.50
[N II]λ6584	15.50±0.43
[S II]λ6717	2.91±0.09
[S II]λ6731	2.94±0.09

Table 5. Gaussian components of Hα profile fit

Feature	FWHM [Å]
Hα$_{verybroad}$	253± 35
Hα$_{broad}$	78± 3
[N II]λ6548	7.2±1.5
Hα$_{narrow}$	8.1±1.3
[N II]λ6584	8.9±0.7

Table 6. The parameters R_{max} and F_{var} of the emission lines Hα and Hβ, of the continuum flux F_{6310} and of the B-band flux as well as corrected for narrow line contributions.

Feature	R_{max}	F_{var}	R_{max}^{corr}	F_{var}^{corr}
Hα complex	1.65	0.107	1.75	0.122
Hβ complex	2.00	0.152	2.05	0.159
F_{6310}	1.68	0.068	...	...
F_{Bband}	1.49	0.072	...	...

ences between the corrected and uncorrected values are of the order of 5%. Both parameters R_{max} and F_{var} indicate that Hβ varies with a larger relative amplitude than Hα.

3.2. Continuum light curves

3.2.1. Continuum B-band light curve

The best temporal coverage of the photometric campaign was achieved in the B and I bands. The image field of NGC 4593 contains two stars. Measurements of their relative fluxes can be used for calibration of the nucleus of NGC 4593. Star 1 is located at a distance of 125″ from the nucleus and at a position angle of 306° while star 2 is separated by 178″ at a position angle of 297°. The flux of the active nucleus and of the stars was measured through a circular aperture with a diameter of 10″. Star 2 is 4 magnitudes brighter than star 1. The flux ratio of the two stars was constant within 3 %. The relative normalized flux of the nucleus of NGC 4593 in the B-band with respect to star 2 given in Table 3 is displayed in Fig. 6.
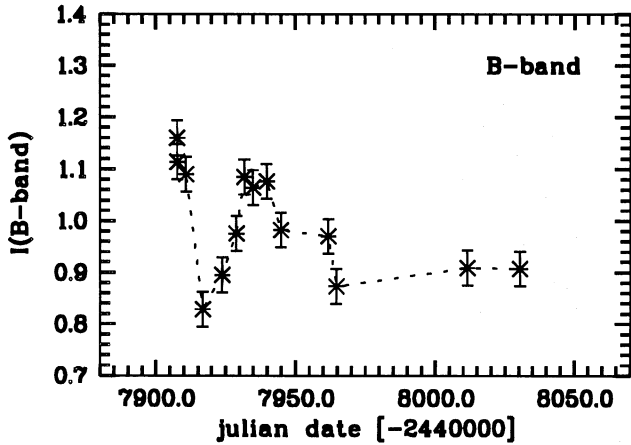
half of January was not sampled by our observations of the Hβ emission line (Fig. 5).

The amplitude of the emission line variations can be characterized by R_{max} and F_{var} as defined by Clavel et al. (1991). These parameters give the ratio of the maximum to minimum flux and the rms of the fluctuations relative to the mean flux, respectively. The values of R_{max} and F_{var} for the Hα and Hβ emission lines are given in Table 6 as well as the values after correction with respect for the narrow line fluxes. The differ-

Fig. 6. Continuum light curve of the relative B band flux. The flux is normalized to the mean flux
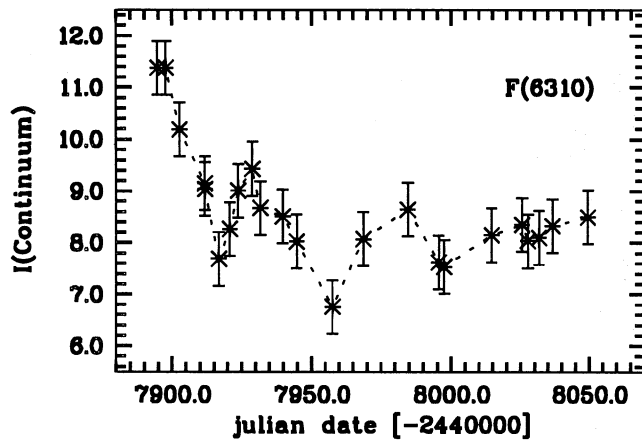
Fig. 7. Continuum light curve at $\lambda = 6310$ Å. The flux is given in units of 10^{-15} erg s^{-1} cm^{-2} Å^{-1}

The pattern of variability is similar in the other colour bands. Since the measurements were not corrected for the underlying stellar contribution the amplitude of the variations increased to shorter wavelengths. For this reason and because of the completeness of the data compared with the other bands we used the B-band light curve for comparison with the variable continuum derived from the spectra.

3.2.2. Continuum light curve F_{6310} from the spectra

We derived a continuum light curve using the spectra containing the Hα emission line. The stellar component of NGC 4593 contributes significantly to the total continuum flux (Crenshaw & Peterson 1985). The continuum flux F_{6310} was measured in the wavelength range from 6300 to 6320 Å, corresponding to 6250 to 6270 Å in the restframe of NGC 4593. This wavelength range is not contaminated by strong emission lines. We integrated the flux over this wavelength range and compared the spatial distributions of the continuum flux at different epochs. This continuum flux is a combination of the constant stellar com-

ponent and the variable central nonthermal component. Since the spectra were always taken at the same position angle the stellar component originated in the same part of the galaxy. The 2D-light distribution of all our observing epochs was calibrated with respect to the outer parts of the galaxy at a distance of 5 to 10 arcsec from the centre, which is assumed to be constant. We measured the continuum flux, which is composed of a variable and a constant flux component, in the central 3 arcsec of the spatial profile. The constant stellar light contribution of the underlying galaxy did not effect the time scales of the variation. Only the amplitude of the variability is reduced. The light loss in the direction perpendicular to the slit is seeing dependent. We estimated this effect by comparison with simulations made by Wanders et al. (1992) and Salamanca et al. (1993). The resulting continuum light curve is shown in Fig. 7. The parameters R_{max} and F_{var} of the F_{6310} continuum flux variations are given in Table 6.

4. Time series analysis

Initial estimates of the size and structure of the broad-line region can be obtained from the emission-line and continuum cross-correlation functions (CCF) and the auto-correlation functions (ACF) (e.g. Gaskell & Peterson 1987; Maoz & Netzer 1989; Robinson & Pérez 1990; Pérez et al. 1992). We computed the ACFs and CCFs in the same way as described by Dietrich et al. (1993).

4.1. The auto-correlation function of the sampling window

First we computed the auto-correlation function of the sampling window, ACF$_{SW}$, for the Hα and Hβ light curves. The observed ACF is given by the convolution of ACF$_{SW}$ and the intrinsic ACF, i.e. the ACF of a perfectly sampled time series (Gaskell & Peterson 1987). Therefore, we sampled white noise with the same temporal distribution as the epochs of the measurements. Then the auto-correlation function of this time series was calculated. The procedure was repeated several thousand times. Finally, the average of all ACFs resulted in the ACF$_{SWs}$ for the light curves. From the width of this function the influence of the interpolation process on the auto-correlation function can be estimated. The auto-correlation functions of the sampling windows for Hα and Hβ are shown in Fig. 8 and 9. The FWHM of the ACF$_{SWs}$ was 6.0 days for Hα and 14.3 days for Hβ.

4.2. The ACF of the light curves

The auto-correlation function of the Hα and Hβ light curves as well as the ACF of the continuum F_{6310} are shown in Fig. 8–10. The sampling of a variation is considered to be sufficient if

$$\text{HWHM(ACF}_{sw}) \leq 1.1 \text{ HWHM(ACF}_{cont})$$

(Gaskell & Peterson 1987; Koratkar & Gaskell 1991c). For the continuum we find that HWHM(ACF$_{sw}$) = 0.3 HWHM(ACF$_{cont}$) and the interpolation error is less than 5 %. The narrower sampling window AFC$_{sw}$ compared to the line
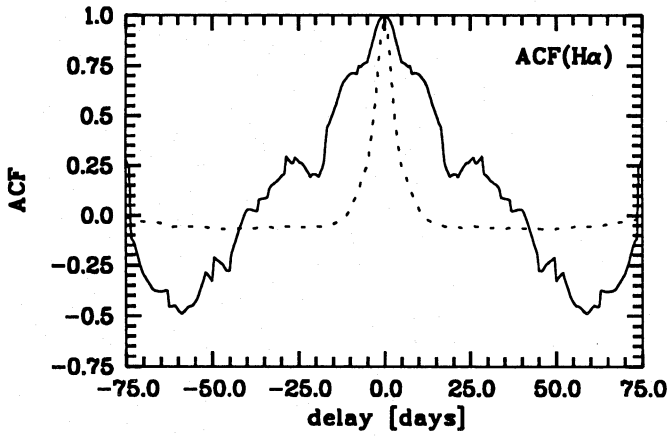
Fig. 8. The auto-correlation function ACF (solid line) and the auto-correlation function of the sampling window ACF$_{SW}$ (dotted line) of Hα. The ACF$_{SW}$ was computed by repeatedly sampling a white noise spectrum in the same pattern as the real observations and computing the auto-correlation function for the sampled data
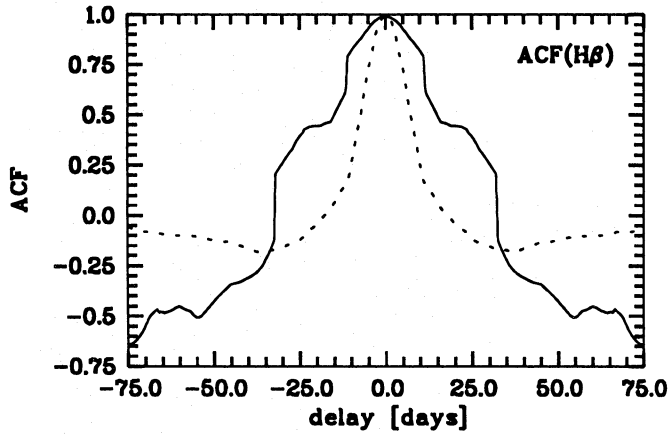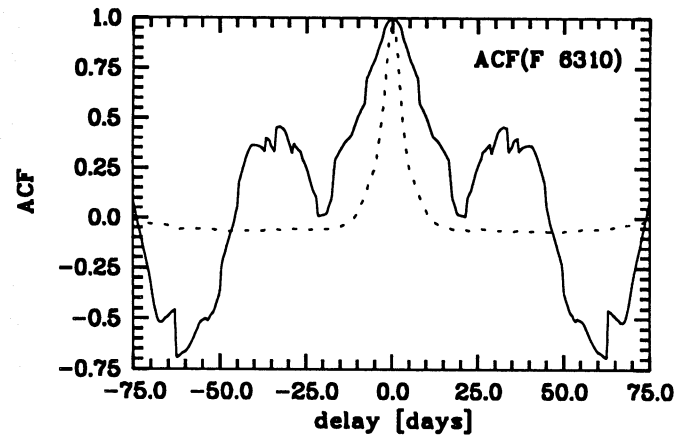

Fig. 10. The auto-correlation function ACF (solid line) and the auto-correlation function of the sampling window ACF$_{SW}$ (dotted line) of the continuum flux F_{6310}

Fig. 9. The auto-correlation function ACF (solid line) and the auto-correlation function of the sampling window ACF$_{SW}$ (dotted line) of Hβ
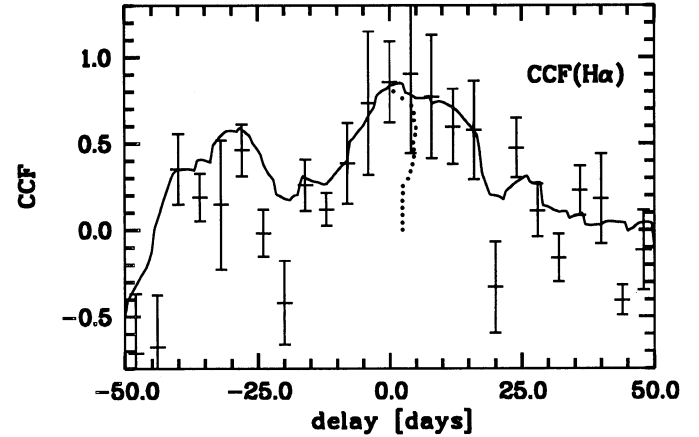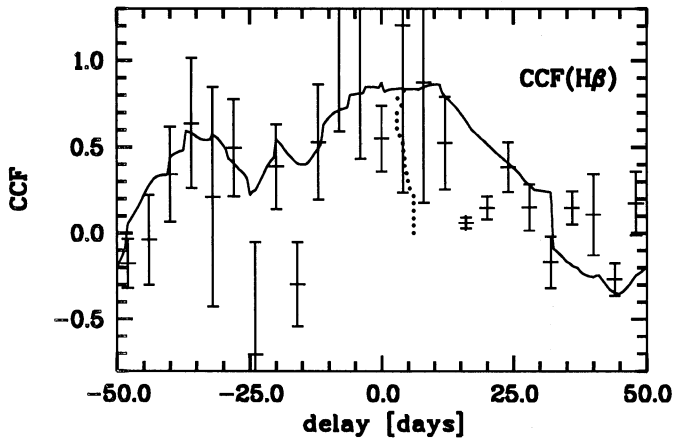

Fig. 11. Cross-correlation function CCF (solid line) and the DCF of the Hα emission line. In addition, the centroid of the CCF for various fractions of the maximum correlation coefficient (dotted) is displayed

and continuum ACFs shows that the dominant part of the power spectrum is being sampled adequately. We therefore claim that NGC 4593 data considered here are reasonably well sampled and the CCF technique can be applied. The coverage of Hβ is slightly worse compared with Hα. We determined an upper limit to the BLR size by measuring the width of the ACFs. The half width at zero intensity (HWZI) of the Hα and Hβ ACF gives an upper limit of 32 to 41 light days for the size of the BLR in NGC 4593. The results of the ACF analysis are summarized in Table 7: Column (2) and (3) list the FWHM and HWZI of the line and continuum ACFs, column (4) and (5) those of the ACF$_{SW}$ of the sampling windows.

4.3. Cross-correlation functions

We cross-correlated the light curves of the Hα and Hβ emission lines with the optical continuum flux at $\lambda_{obs} = 6310$ Å. This

spectral continuum light curve was used since the temporal coverage is better than that of the B-band observations especially for the second half of the monitoring period. The

cross-correlation of the two continuum light curves gave a lag of 1.6±2.9 days which is consistent with zero lag.

The CCFs of the Hα and Hβ emission lines have well defined peaks (Fig. 11 and 12). The maxima of the CCFs of the emission lines were measured by fitting a Gaussian curve to the top of the CCF starting at 70% of its maximum. This procedure gave a peak position of the gaussian fit of $\tau_{max} = 3.3$ days for Hα and $\tau_{max} = 3.3$ days for Hβ. The uncertainties on the positions of τ_{max}, listed as σ_{GP} and σ_{CCPD} (cf. Tab. 8) were calculated using equation (4) given by Gaskell & Peterson (1987) and the cross-correlation peak distribution function as proposed by Maoz & Netzer (1989). The continuum and emission line light curve were fit with a cubic spline and the observed number of epochs were randomly distributed over the time of the monitoring campaign. For these simulated light curves the cross-correlation function was calculated several thousand times. The

Table 7. Results of the ACF analysis in units of days of the $H\alpha$ and $H\beta$ emission lines and of the continuum flux F_{6310} and the corresponding ACF_{SW}.

Feature	(2) FWHM	(3) HWZI	(4) FWHM	(5) HWZI
$H\alpha$	30.2	40.8	6.0	11.3
$H\beta$	29.7	32.3	14.3	17.9
F_{6310}	20.4	19.6	6.0	11.3

Table 8. Results of the CCF analysis of the line vs. continuum light curves in units of days :

Feature	FWHM	τ_{max}	CCF_{max}	σ_{GP}	σ_{CCPD}
$H\alpha$	25.0	3.3	0.85	1.9	3.1
$H\beta$	36.2	3.3	0.87	3.8	12.6

	0.0	0.3	0.6	mean	C
$H\alpha$	2.4	2.5	4.5	4.1±0.8	0.99
$H\beta$	6.0	5.3	3.9	4.3±0.9	0.94

Fig. 12. Cross-correlation function CCF (solid line) and the DCF of the $H\beta$ emission line. In addition, the centroid of the CCF for various fractions of the maximum correlation coefficient (dotted) is displayed

Fig. 13. Normalized $H\alpha$ spectra at the beginning of the campaign, at the minimum state and the corresponding difference spectrum

σ_{CCPD} was estimated from the FWHM of the cross-correlation peak distribution function. The centroids of the CCFs were determined in steps of 5% of the maximum value (cf. Fig. 11 and 12). The columns in Table 8 labelled 0.0, 0.3 and 0.6 refer to the centroids of the CCF obtained by using the values higher than 0%, 30% and 60%, respectively, of the maximum of the CCF. The mean is the average of the centroids of the CCF calculated for fractions of the peak ranging from 25% to 80 % of the maximum value of the cross-correlation function. The CCF analysis provides a lag of 4.1±0.8 days ($H\alpha$) and 4.3±0.9 days ($H\beta$) for the CCF centroid of these emission lines. The confidence level C of the cross-correlation function calculated in the same way as described by Koratkar & Gaskell (1991a) is very high: 0.99 for $H\alpha$ and 0.94 for $H\beta$. The results of the cross-correlation analysis are summarized in Table 8.

We also computed the discrete correlation function (DCF) proposed by Edelson & Krolik (1988) for comparsion with the interpolated CCF as an additional test of the effects of interpolation. For the $H\alpha$ line the DCF gives nearly the same result as the interpolated CCF and even for $H\beta$ both correlation functions are comparable. For well sampled time series the CCF and DCF methods give results which are in good agreement. But it is also known that the DCF method can fail to find a real correlation between two marginally sampled light curves (Peterson 1993).

The centroids of the CCFs of the two Balmer lines can be taken as an estimation for the luminosity weighted radius (Ko-
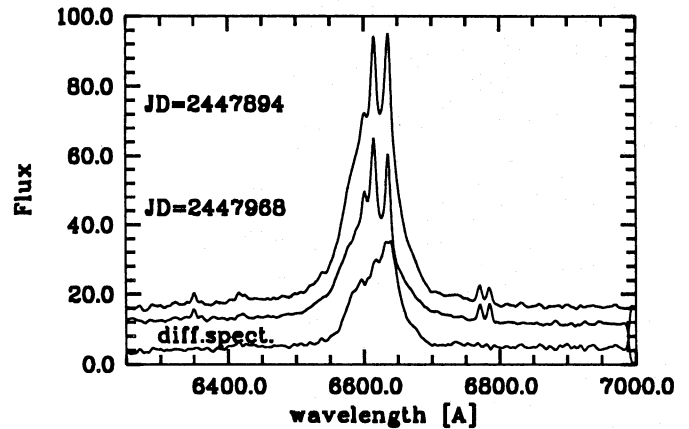
ratkar & Gaskell 1991a; Pérez et al. 1992) while the lag can be taken as a measure of the inner radius of the BLR for a well sampled light curve. The results of the LAG monitoring campaign of NGC 4593 indicate that the size of the BLR might be less than 10 light days. But one has to take into account that the results of cross-correlation function analysis depend strongly on the width and location of the data window (Pérez et al. 1992). Even for a data window which is short in comparison to the variability time scale it is possible to underestimate the size of the BLR. Furthermore, the history of the continuum variations influences the properties of the CCF and also of the ACF. For the Seyfert 1 galaxy NGC 5548 it has been shown that the response time of the optical and UV emission lines depends on the continuum variability time scale (Netzer & Maoz 1990; Netzer et al. 1990; Dietrich 1991).

We compared the size of the BLR which is given by the CCF analysis and the luminosity of the nucleus of NGC 4593 ($\log F_{5500}$ erg s^{-1} cm^{-2} $Å^{-1} = 39.1$) with results of other monitoring campaigns (Maoz et al. 1990, 1991; Peterson et al. 1992; Dietrich et al. 1993; Peterson et al. 1993; Salamanca et al. 1993; Wanders et al. 1993). The trend is confirmed that those Seyfert nuclei with lower intrinsic luminosity have smaller extension of the broad-line region and vice versa (cf. Koratkar & Gaskell 1991b; Peterson 1993). Deviations from this trend may be due to the dependence of the response time from the time scale of the continuum variability.
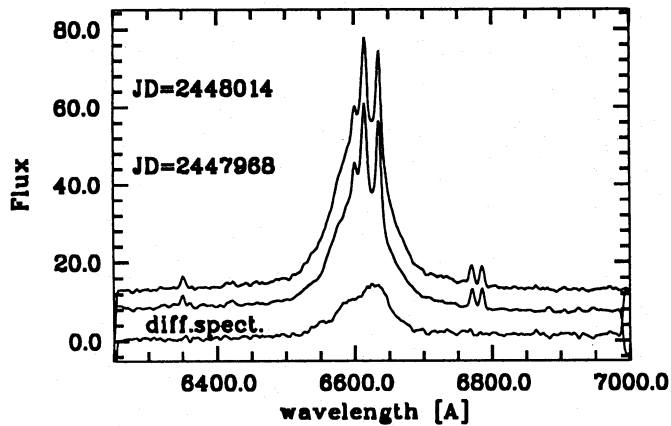
Fig. 14. Normalized Hα spectra at the second half of the campaign, at the minimum state and the corresponding difference spectrum

5. Line profile variations

We have determined difference spectra with respect to the minimum state (JD=2447968) of this monitoring campaign. The narrow emission line fluxes of [OI]λ6300, [NII]$\lambda\lambda$6548,6584, Hα_{narrow}, and [SII]$\lambda\lambda$6717,6731 were used to intercalibrate the variable broad emission line flux of Hα. The narrow emission line flux was assumed to be constant and hence was cancelled out in difference spectra (cf. Fig. 13,14). Fig. 13 shows a spectrum at the beginning of the campaign (JD=2447894), in the low state (JD=2447968), and the corresponding difference spectrum. Spectra at the second half of the campaign (JD=2448014) and at epoch JD=2447968 are displayed in Fig. 14. Both difference spectra of the Hα line are asymmetric with respect to the blue wing of the profile. The FWZI of the difference spectra is constant and amounts to FWZI=9000 km s^{-1}. Furthermore, at least three substructures can be detected in the difference profile. A strong component which is shifted to the red with v^I=500 km s^{-1} and two blue components at $v^{II} = -1000$ km s^{-1} and $v^{III} = -3000$ km s^{-1}. The relative velocities were calculated with respect to the redshift of the narrow emission lines. A detailed discussion of the kinematics and the temporal evolution of the broad Hα and Hβ emission line profiles of NGC 4593 will be given in a subsequent paper (Kollatschny et al. 1993).

6. Summary

The Seyfert 1 galaxy NGC 4593 was monitored in the optical from January until June 1990. Spectra for Hα at 22 epochs and for Hβ at 11 epochs were obtained using the 4.2m and the 2.5m telescopes at La Palma. During this monitoring campaign variations on time scales of weeks to days were detected for the Hα and Hβ emission lines. From January until mid March the integrated Hα emission line flux declined by 60 %. Furthermore, in January a short term variability event was superimposed on this decreasing flux. Within 5 days the Hα emission line flux decreased by 30 %.

We have applied time series analysis methods to the light curves of the emission lines and of the continuum flux. We

derived an upper limit of 30 – 40 light days for the size of the BLR of NGC 4593 from the auto-correlation function. The cross-correlation of the emission lines and the varying continuum shows that the variations of the line fluxes are delayed with respect to the continuum variations. Using the centroid of the cross-correlation functions we get a luminosity weighted radius of the BLR of 4.1 (Hα) and 4.3 (Hβ) light days, respectively. This indicates that NGC 4593 may have a compact BLR.

The result of the NGC 4593 monitoring campaign supports the trend that Seyfert nuclei with lower intrinsic luminosity have smaller extension.

References

Andrillat, Y. and Souffrin, S., 1968, ApL 1, 111
Barnes, J.V. and Hayes, D.S., 1984, KPNO IRS Standard Star Manual
Barr, P., Clavel, J., Giommi, P., Mushotzky, R.F. and Madejski, G., 1987, in Aldo Treves (ed.), Associazione per l'Avanzamento dell'Astronomia, 'Variability of Galactic and Extragalactic X-ray sources', p.43
Clavel, J., Joly, M., Collin-Souffrin, S., Bergeron, J. and Penston, M.V., 1983, MNRAS 202, 85
Clavel, J., 1983, MNRAS 204, 189
Clavel, J., Boksenberg, A., Bromage, G.E., et al., 1990, MNRAS 246, 668
Clavel, J., Reichert, G.A., Alloin, D., et al., 1991, ApJ 366, 64
Crenshaw, D.M. and Peterson, B.M., 1985, ApJ 291, 677
Dibaj, E.A. and Pronik, V.I., 1967, AZh 44, 952
Dietrich, M., PhD thesis, 1991, University of Göttingen
Dietrich, M., Kollatschny, W., Peterson, B.M., et al., 1993, ApJ 408, 416
Edelson, R.A. and Krolik, J.H., 1988, ApJ 333, 646
Gaskell, C.M. and Peterson, B.M., 1987, ApJS 67, 1
Jackson, N., O'Brien, P.T., Goad, M.R., et al., 1992, A&A 262, 17
Kollatschny, W. and Fricke, K.J., 1985, A&A 143, 393
Kollatschny, W. and Fricke, K.J., 1989, A&A 219, 34
Kollatschny et al., 1993 in prep.
Koratkar, A. and Gaskell, C.M., 1991a, ApJS 75, 719
Koratkar, A. and Gaskell, C.M., 1991b, ApJ 370, L61
Koratkar, A. and Gaskell, C.M., 1991c, ApJ 375, 85
Maoz, D. and Netzer, H., 1989, MNRAS 236, 21
Maoz, D., Netzer, H., Leibowitz, E., et al., 1990, ApJ 351, 75
Maoz, D., Netzer, H., Mazeh, T., et al., 1991, ApJ 367, 493
Netzer H., Maoz, D., Laor, A., et al., 1990, ApJ 353, 108

Netzer, H. and Maoz, D., 1990, ApJ 365, L5

Oke, J.B. and Gunn, J.E., 1983, ApJ 266, 713

Oke, J.B., 1990, AJ 99, 1621

Pérez, E., Robinson, A. and de la Fuente, L., 1992, MNRAS 255, 502

Peterson, B.M., Crenshaw, D.M., and Meyers, K.A., 1985, ApJ 298, 283

Peterson, B.M., et al., 1991, ApJ 368, 119

Peterson, B.M., Alloin, D., Axon, D., et al., 1992, ApJ 392, 470

Peterson, B.M., Ali, B., Horne, K., et al., 1993, ApJ 402, 469

Peterson, B.M., 1993, PASP, 105, 247

Robinson, A. and Pérez, E., 1990, MNRAS 244, 138

Salamanca, I., Alloin, D., Baribaud, T., et al., 1993, A&A, in press

Santos-Lleó, M., Clavel, J., Barr, P. and Glass, I.S., 1990, in 'Evolution in Astrophysics', Toulouse, ESA-SP310, p.539

van Groningen, E. and Wanders, I., 1992, PASP 104, 700

van Groningen, E. and Wanders, I., 1993, in proc. 'The Nature of the Compact Object in AGN', Cambridge, in press

Véron-Cetty, M.-P. and Veron, P., 1991, A Catalogue of Quasars and Active Nuclei, 5. Edition

Wanders, I., Peterson, B.M., Pogge, R.W., DeRobertis, M.M. and van Groningen, E., 1992, A&A 266, 72

Wanders, I., van Groningen, Alloin, D., et al., 1993, 1993, A&A 269, 39

Whittle, M., 1992, ApJS 79, 49